

Constraining and applying a generic high-density equation of state

Mark G. Alford¹, G. F. Burgio², S. Han (韓君)¹, G. Taranto^{2,3}, and D. Zappalà²

¹*Physics Department, Washington University, Saint Louis, Missouri 63130, USA*

²*INFN Sezione di Catania, Via Santa Sofia 64, 95123 Catania, Italy and*

³*Dipartimento di Fisica e Astronomia, Università di Catania, Via Santa Sofia 64, 95123 Catania, Italy*

(Dated: 1 Oct 2015)

We discuss the “constant speed of sound” (CSS) parametrization of the equation of state of high-density matter and its application to the field correlator method (FCM) model of quark matter. We show how observational constraints on the maximum mass and typical radius of neutron stars are expressed as constraints on the CSS parameters. We find that the observation of a $2M_{\odot}$ star already severely constrains the CSS parameters, and is particularly difficult to accommodate if the squared speed of sound in the high-density phase is assumed to be around 1/3 or less.

We show that the FCM equation of state can be accurately represented by the CSS parametrization, which assumes a sharp transition to a high-density phase with density-independent speed of sound. We display the mapping between the FCM and CSS parameters, and see that FCM only allows equations of state in a restricted subspace of the CSS parameters.

PACS numbers: 25.75.Nq, 26.60.-c, 97.60.Jd

I. INTRODUCTION

There are many models of matter at density significantly above nuclear saturation density, each with their own parameters. In studying the equation of state (EoS) of matter in this regime it is therefore useful to have a general parametrization of the EoS which can be used as a generic language for relating different models to each other and for expressing experimental constraints in model-independent terms. In this work we use the previously proposed “constant speed of sound” (CSS) parametrization [1–3] (for applications, see, e.g., [4]). We show how mass and radius observations can be expressed as constraints on the CSS parameters. Here we analyze a specific example, where the high-density matter is quark matter described by a model based on the field correlator method (Sec. IV), showing how its parameters can be mapped on to the CSS parameter space, and how it is constrained by currently available observations of neutron stars.

The CSS parametrization is applicable to high-density equations of state for which (a) there is a sharp interface between nuclear matter and a high-density phase which we will call quark matter, even when (as in Sec. II) we do not make any assumptions about its physical nature; and (b) the speed of sound in the high-density matter is pressure-independent for pressures ranging from the first-order transition pressure up to the maximum central pressure of neutron stars. One can then write the high-density EoS in terms of three parameters: the pressure p_{trans} of the transition, the discontinuity in energy density $\Delta\epsilon$ at the transition, and the speed of sound c_{QM} in the high-density phase. For a given nuclear matter EoS $\epsilon_{\text{NM}}(p)$, the full CSS EoS is then

$$\epsilon(p) = \begin{cases} \epsilon_{\text{NM}}(p) & p < p_{\text{trans}} \\ \epsilon_{\text{NM}}(p_{\text{trans}}) + \Delta\epsilon + c_{\text{QM}}^{-2}(p - p_{\text{trans}}) & p > p_{\text{trans}} \end{cases} \quad (1)$$

The CSS form can be viewed as the lowest-order terms of a Taylor expansion of the high-density EoS about the transition pressure. Following Ref. [1], we express the three

parameters in dimensionless form, as $p_{\text{trans}}/\epsilon_{\text{trans}}$, $\Delta\epsilon/\epsilon_{\text{trans}}$ (equal to $\lambda - 1$ in the notation of Ref. [5]) and c_{QM}^2 , where $\epsilon_{\text{trans}} \equiv \epsilon_{\text{NM}}(p_{\text{trans}})$.

The assumption of a sharp interface will be valid if, for example, there is a first-order phase transition between nuclear and quark matter, and the surface tension of the interface is high enough to ensure that the transition occurs at a sharp interface (Maxwell construction) not via a mixed phase (Gibbs construction). Given the uncertainties in the value of the surface tension [6–8], this is a possible scenario. One can also formulate generic equations of state that model interfaces that are smeared out by mixing or percolation [9–11].

The assumption of a density-independent speed of sound is valid for a large class of models of quark matter. The CSS parametrization is an almost exact fit to some Nambu–Jona–Lasinio models [2, 12–14]. The perturbative quark matter EoS [15] also has roughly density-independent c_{QM}^2 , with a value around 0.2 to 0.3 (we use units where $\hbar = c = 1$), above the transition from nuclear matter (see Fig. 9 of Ref. [16]). In the quartic polynomial parametrization [17], varying the coefficient a_2 between $\pm(150\text{MeV})^2$, and the coefficient a_4 between 0.6 and 1, and keeping n_{trans}/n_0 above 1.5 ($n_0 \equiv 0.16\text{ fm}^{-3}$ is the nuclear saturation density), one finds that c_{QM}^2 is always between 0.3 and 0.36. It is noticeable that models based on relativistic quarks tend to have $c_{\text{QM}}^2 \approx$ close to 1/3, which is the value for systems with conformal symmetry, and it has been conjectured that there is a fundamental bound $c_{\text{QM}}^2 < 1/3$ [18], although some models violate that bound, e.g. [19, 20] or [14] (parametrized in [2]).

In Sec. II we show how the CSS parametrization is constrained by observables such as the maximum mass M_{max} , the radius of a maximum-mass star, and the radius $R_{1.4}$ of a star of mass $1.4M_{\odot}$. In Secs. III–IV we describe a specific model, based on a Brueckner–Hartree–Fock (BHF) calculation of the nuclear matter EoS and the field correlator method (FCM) for the quark matter EoS. We show how the parameters of this model map on to part of the CSS parameter space, and how the observational constraints apply to the FCM model param-

eters. Section V gives our conclusions.

II. CONSTRAINING THE CSS PARAMETERS

A. Topology of the mass-radius relation

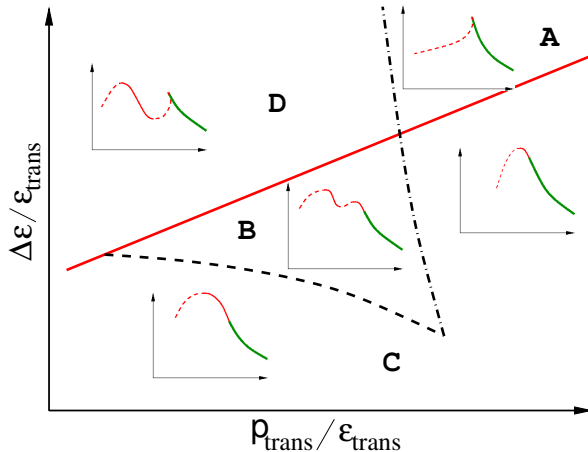


FIG. 1: (Color online). Schematic phase diagram (from [1]) for hybrid star branches in the mass-radius relation of compact stars. We fix c_{QM}^2 and vary $p_{trans}/\epsilon_{trans}$ and $\Delta\epsilon/\epsilon_{trans}$. The four regions are (A) no hybrid branch (“absent”); (B) both connected and disconnected hybrid branches; (C) connected hybrid branch only; and (D) disconnected hybrid branch only.

We use the term “hybrid star” to refer to stars whose central pressure is above p_{trans} , and so they contain a core of the high-density phase. The part of the mass-radius relation that arises from such stars is the hybrid branch. In all models of nuclear/quark matter we find the same four topologies of the mass-radius curve for compact stars: the hybrid branch may be connected to the nuclear branch (C), or disconnected (D), or both may be present (B) or neither (A). The occurrence of these as a function of the CSS parameters $p_{trans}/\epsilon_{trans}$ and $\Delta\epsilon/\epsilon_{trans}$ at fixed c_{QM}^2 is shown schematically in Fig. 1 (taken from Ref. [1]). The mass-radius curve in each region is depicted in inset plots, in which the thick green line is the hadronic branch, the thin solid red lines are stable hybrid stars, and the thin dashed red lines are unstable hybrid stars.

In the phase diagram the solid red line shows the threshold value $\Delta\epsilon_{crit}$ below which there is always a stable hybrid star branch connected to the neutron star branch. This critical value is given by [5, 21, 22]

$$\frac{\Delta\epsilon_{crit}}{\epsilon_{trans}} = \frac{1}{2} + \frac{3}{2} \frac{p_{trans}}{\epsilon_{trans}} \quad (2)$$

and was obtained by performing an expansion in powers of the size of the core of high-density phase. Equation (2) is an analytic result, independent of c_{QM}^2 and the nuclear matter EoS. The dashed and dot-dashed black lines mark the border of regions where the disconnected hybrid star branch exists.

The position of these lines depends on the value of c_{QM}^2 and (weakly) on the accompanying nuclear matter EoS [1].

Once a nuclear matter EoS has been chosen, any high-density EoS that is well approximated by the CSS parametrization can be summarized by giving the values of the three CSS parameters, corresponding to a point in the phase diagram. We then know what sort of hybrid branches will be present.

B. Maximum mass of hybrid stars

Property	BHF, Av ₁₈ + UVIX TBF	DBHF, Bonn A
Saturation baryon density n_0 (fm ⁻³)	0.16	0.18
Binding energy/baryon E/A (MeV)	-15.98	-16.15
Compressibility K_0 (MeV)	212.4	230
Symmetry energy S_0 (MeV)	31.9	34.4
$L = 3n_0 [dS_0/dn]_{n_0}$ (MeV)	52.9	69.4
Maximum mass of star (M_\odot)	2.03	2.31
Radius of the heaviest star (km)	9.92	11.26
Radius of $M = 1.4 M_\odot$ star (km)	11.77	13.41

TABLE I: (Color online). Calculated properties of symmetric nuclear matter for the BHF and Dirac-Brueckner-Hartree-Fock (DBHF) nuclear equations of state used here. BHF is softer, and DBHF is stiffer (see Sec. III)

In Fig. 2 we show how mass measurements of neutron stars can be expressed as constraints on the CSS parameters. Each panel shows dependence on $p_{trans}/\epsilon_{trans}$ and $\Delta\epsilon/\epsilon_{trans}$ for fixed c_{QM}^2 , as in Fig. 1. The region in which the transition to quark matter would occur below nuclear saturation density ($n_{trans} < n_0$) is excluded (hatched band at the left end) because in that region bulk nuclear matter would be metastable. There is also an upper limit on the transition pressure, which is the central pressure of the heaviest stable nuclear matter star. This depends on the hadronic EoS that had been assumed.

The contours show the maximum mass of a hybrid star as a function of the EoS parameters. The region inside the $M = 2M_\odot$ contour corresponds to EoSes for which the maximum mass is less than $2M_\odot$ so it is shaded to signify that this region of parameter space for the high-density EoS is excluded by the observation of a star with mass $2M_\odot$ [23]. For high-density EoSs with $c_{QM}^2 = 1$ (right-hand plots), this region is not too large, and leaves a good range of transition pressures and energy density discontinuities that are compatible with the observation. However, for high-density matter with $c_{QM}^2 = 1/3$ (left-hand plots), which is the typical value in many models (See Sec. I), the $M_{max} > 2M_\odot$ constraint eliminates a large region of the CSS parameter space [1, 18]. We discuss this in more detail below.

The upper plots in Fig. 2 are for a stiffer nuclear matter EoS, DBHF[24], and the lower plots are for a softer nuclear matter EoS, BHF [25] (see Sec. III). Properties of these nuclear matter EoSs are given in Table I. As one would expect, the stiffer EoS gives rise to heavier (and larger) stars, and therefore al-

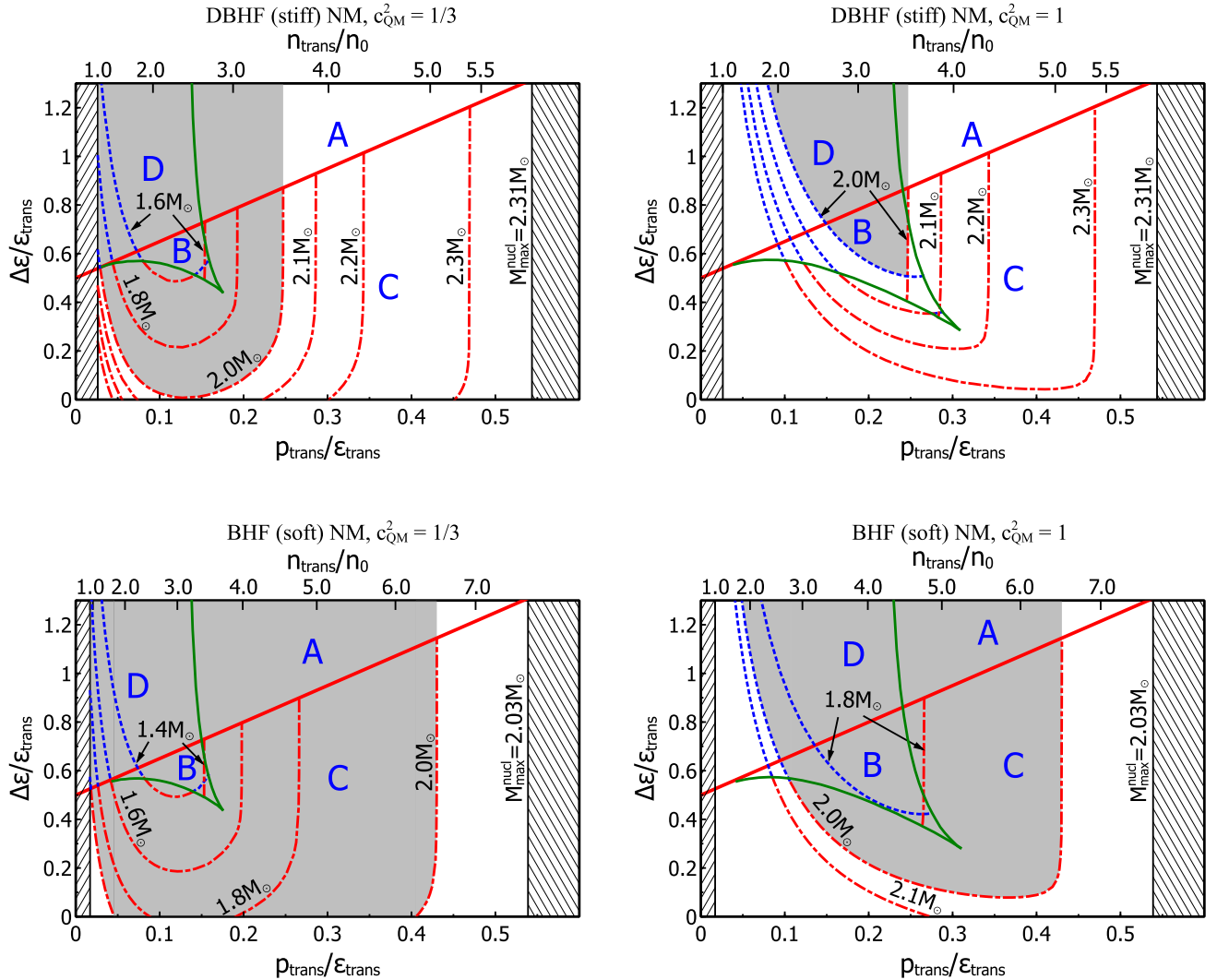


FIG. 2: (Color online). Contour plots showing the maximum hybrid star mass as a function of the CSS parameters of the high-density EoS. Each panel shows the dependence on the CSS parameters $p_{\text{trans}}/\epsilon_{\text{trans}}$ and $\Delta\epsilon/\epsilon_{\text{trans}}$. The left plots are for $c_{\text{QM}}^2 = 1/3$, and the right plots are for $c_{\text{QM}}^2 = 1$. The top row is for a DBHF (stiff) nuclear matter EoS, and the bottom row is for a BHF (soft) nuclear matter EoS. The grey shaded region is excluded by the measurement of a $2M_{\odot}$ star. The hatched band at low density (where $n_{\text{trans}} < n_0$) is excluded because bulk nuclear matter would be metastable. The hatched band at high density is excluded because the transition pressure is above the central pressure of the heaviest stable hadronic star.

lows a wider range of CSS parameters to be compatible with the $2M_{\odot}$ measurement.

In Fig. 2 the dot-dashed (red) contours are for hybrid stars on a connected branch, while the dashed (blue) contours are for disconnected branches. As discussed in Ref. [1], when crossing the near-horizontal boundary from region C to B the connected hybrid branch splits into a smaller connected branch and a disconnected branch, so the maximum mass of the connected branch smoothly becomes the maximum mass of the disconnected branch. Therefore the red contour in the C region smoothly becomes a blue contour in the B and D regions. When crossing the near-vertical boundary from region C to B a new disconnected branch forms, so the connected branch (red dot-dashed) contour crosses this boundary

smoothly.

In each panel of Fig. 2, the physically relevant allowed region is the white unshaded region. The grey shaded region is excluded by the existence of a $2M_{\odot}$ star. We see that increasing the stiffness of the hadronic EoS or of the quark matter EoS (by increasing c_{QM}^2) shrinks the excluded region.

For both the hadronic EoSs that we study, the CSS parameters are significantly constrained. From the two left panels of Fig. 2 one can see that if, as predicted by many models, $c_{\text{QM}}^2 \lesssim 1/3$, then we are limited to two regions of parameter space, corresponding to a low-pressure transition or a high-pressure transition. In the low-transition-pressure region the transition occurs at a fairly low density $n_{\text{trans}} \lesssim 2n_0$, and a connected hybrid branch is possible. In the high-transition-

pressure region the connected branch (red dot-dashed) contours are, except at very low $\Delta\epsilon$, almost vertical, corresponding to EoSs that give rise to a very small connected hybrid branch which exists in a very small range of central pressures p_{cent} just above p_{trans} . The maximum mass on this branch is therefore very close to the mass of the purely hadronic matter star with $p_{\text{cent}} = p_{\text{trans}}$. The mass of such a purely hadronic star is naturally independent of parameters that only affect the quark matter EoS, such as $\Delta\epsilon$ and c_{QM}^2 , so the contour is vertical. These hybrid stars have a tiny core of the high-density phase and cover a tiny range of masses, of order $10^{-3} M_{\odot}$ or less, and so would be very rare.

Disconnected hybrid branches are of special interest, because they give a characteristic signature in mass-radius measurements. For both the hadronic EoSs that we study, the region B and D, where disconnected hybrid star branches can occur, are excluded for $c_{\text{QM}}^2 \leq 1/3$. Even for larger c_{QM}^2 disconnected branches only arise if the nuclear matter EoS is sufficiently stiff. It is interesting to note that using an extremely stiff hadronic matter EoS such as DD2-EV [26] can further shrink the region that is excluded by the $M_{\text{max}} > 2M_{\odot}$ constraint, allowing disconnected branches of hybrid stars to occur.

C. Minimum radius of hybrid stars

In Fig. 3 we show contour plots of the radius of the maximum-mass star (on either a connected or disconnected hybrid branch) as a function of the CSS quark matter EoS parameters. Since the smallest hybrid star is typically the heaviest one, this allows us to infer the smallest radius that arises from a given EoS.

The layout is as in Fig. 2: each panel shows dependence on $p_{\text{trans}}/\epsilon_{\text{trans}}$ and $\Delta\epsilon/\epsilon_{\text{trans}}$ for fixed c_{QM}^2 ; the plots on the left are for $c_{\text{QM}}^2 = 1/3$ and the plots on the right are for $c_{\text{QM}}^2 = 1$; the plots on the top are for the stiffer DBHF nuclear matter EoS, while the lower plots are for the softer BHF nuclear matter EoS. As in Fig. 2, the region that is eliminated by the observation of a $2M_{\odot}$ star is shaded in grey.

The smallest stars, with radii as small as 9 km, occur when the high-density phase has the largest possible speed of sound $c_{\text{QM}}^2 = 1$. They are disconnected branch stars arising from EoSs having a low transition pressure ($n_{\text{trans}} \lesssim 2n_0$) with a fairly large energy density discontinuity ($\Delta\epsilon/\epsilon_{\text{trans}} \gtrsim 1$).

As in Fig. 2, the contours in the high-transition-pressure region are almost vertical because the hybrid branch is then a very short extension to the nuclear mass-radius relation, and its radius is close to that of the heaviest purely hadronic star, which is independent of $\Delta\epsilon/\epsilon_{\text{trans}}$ and c_{QM}^2 . The radius of the hybrid stars decreases with p_{trans} in this region, because the radius of hadronic stars decreases with central pressure.

For $c_{\text{QM}}^2 = 1/3$, the allowed low-transition-pressure region is disconnected from the high-transition-pressure region and is so small that it is hard to see on this plot. By magnifying it (left-hand plots of Fig. 5) we see that in this region the radius contours closely track the border of the allowed region

(the $M_{\text{max}} = 2M_{\odot}$ line) so we can say that the radius must be greater than 11.5 km almost independent of the transition pressure and hadronic EoS. For a stiff hadronic EoS this minimum is raised to 11.7 km. These values are comparable to the minimum radius of about 11.8 km found in Ref. [18], which explored a larger set of hadronic EoSs but did not explore the full CSS parameter space for the high-density EoS. If a star with radius smaller than this minimum value were to be observed, we would have to conclude that either the transition occurs outside the low-density region or that c_{QM}^2 is greater than 1/3. In the magnified figure we also show how the excluded region would grow if a $2.1M_{\odot}$ star were to be observed (long-dashed line for connected branch stars and short-dashed line for disconnected branch stars). This would increase the minimum radius to about 12.1 km for the soft hadronic EoS and 12.2 km for the stiff hadronic EoS.

D. Typical radius of hybrid stars

In Fig. 4 we show contours (the U-shaped lines) of typical radius of a hybrid star, defined as $R_{1.4}$, the radius of a star of mass $1.4M_{\odot}$, as a function of the CSS quark matter EoS parameters. The contours only fill the part of the CSS parameter space where there are hybrid stars with that mass. The dashed (magenta) lines delimit that region which extends only up to moderate transition pressure.

The overall behavior is that, at fixed $\Delta\epsilon/\epsilon_{\text{trans}}$, the typical radius is large when the transition density is at its lowest. As the transition density rises the radius of a $1.4M_{\odot}$ star decreases at first, but then increases again. This is related to the previously noted fact [27] that when one fixes the speed of sound of quark matter and increases the bag constant (which increases $p_{\text{trans}}/\epsilon_{\text{trans}}$ and also varies $\Delta\epsilon/\epsilon_{\text{trans}}$ in a correlated way) the resultant family of mass-radius curves all pass through the same small region in the M - R plane: the $M(R)$ curves “rotate” counterclockwise around this hub (see Fig. 2 of Ref. [27]). In our case we are varying $p_{\text{trans}}/\epsilon_{\text{trans}}$ at fixed $\Delta\epsilon/\epsilon_{\text{trans}}$, so the hub itself also moves. At low transition density the hub is below $1.4M_{\odot}$, so $R_{1.4}$ decreases with $p_{\text{trans}}/\epsilon_{\text{trans}}$. At high transition density the hub is at a mass above $1.4M_{\odot}$ so $R_{1.4}$ will increase with $p_{\text{trans}}/\epsilon_{\text{trans}}$.

The smallest stars occur for $c_{\text{QM}}^2 = 1$ (right-hand plots), where $R_{1.4} \gtrsim 9.5$ km at large values of the energy density discontinuity, and the radius rises as the discontinuity is decreased. This is consistent with the absolute lower bound of about 8.5 km [28] for the maximally compact $c_{\text{QM}}^2 = 1$ star obeying $M_{\text{max}} > 2M_{\odot}$.

For $c_{\text{QM}}^2 = 1/3$ the allowed region at low transition pressure is small, so in the right panels of Fig. 5 we show a magnification of this region. We see that in the allowed ($M_{\text{max}} > 2M_{\odot}$ and $n_{\text{trans}} > n_0$) region there is a minimum radius 12.2 km for the BHF (soft) hadronic EoS, and about 12.5 km for the DBHF (stiff) hadronic EoS. This minimum is attained at the lowest possible transition density, $n_{\text{trans}} \approx n_0$. As the transition density rises to values around $2n_0$, the minimum radius rises to 12.5 (BHF) or 13.3 km (DBHF). This is comparable to the minimum radius of about 13 km found in Ref. [18],

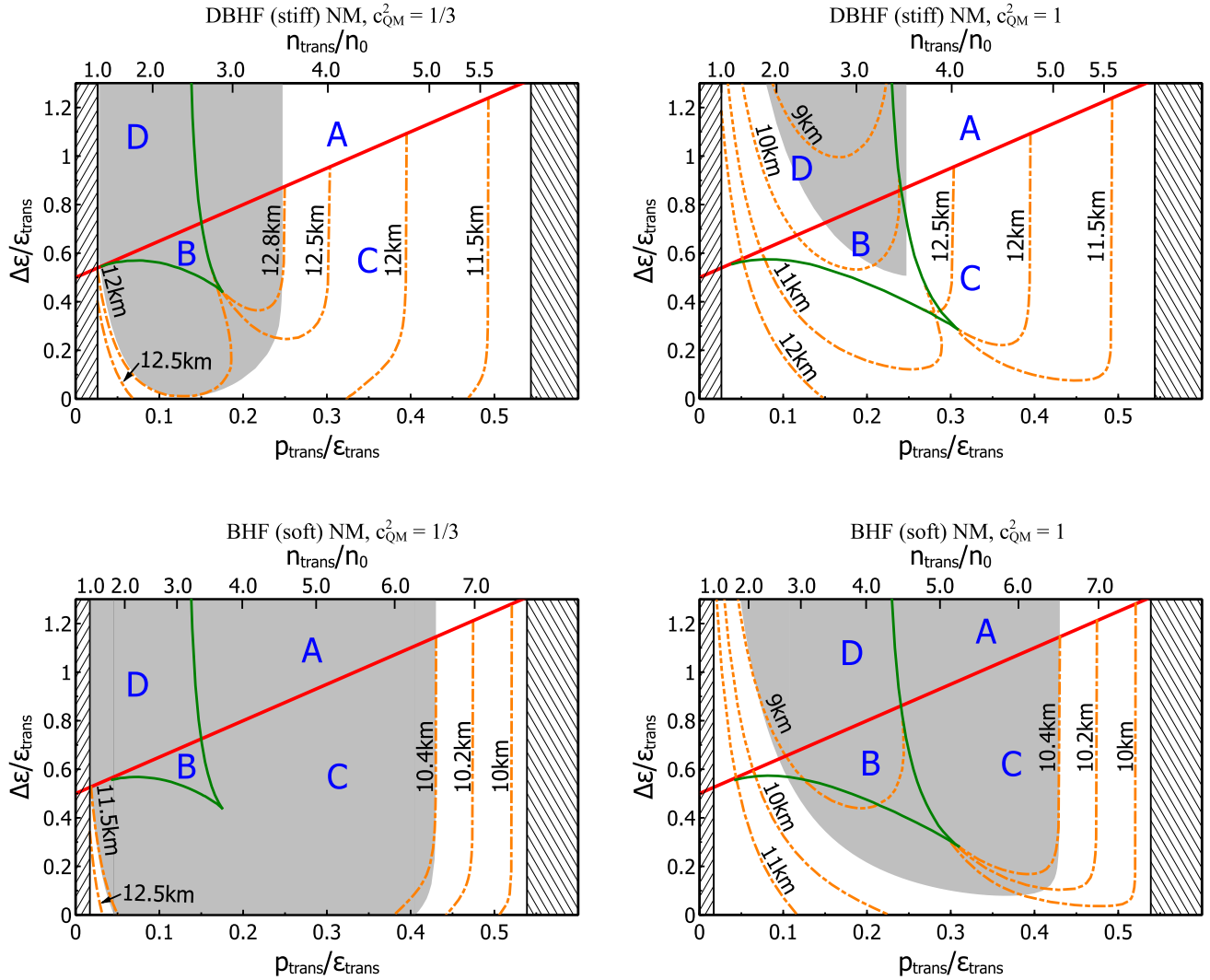


FIG. 3: (Color online). Contour plots showing the radius of the maximum-mass star as a function of the CSS parameters. Dashed lines are for the case where this star is on the disconnected branch; for dot-dashed lines it is on the connected branch. The grey shaded region is excluded by the measurement of a $2M_{\odot}$ star. The hatched band at low density (where $n_{\text{trans}} < n_0$) is excluded because bulk nuclear matter would be metastable. The hatched band at high density is excluded because the transition pressure is above the central pressure of the heaviest stable hadronic star. For a magnified version of the low-transition-pressure region for $c_{\text{QM}}^2 = 1/3$, see Fig. 5.

which explored a wider range of hadronic EoSs but assumed $n_{\text{trans}} = 2n_0$. These results are consistent with the lower bound on $R_{1.4}$ for $c_{\text{QM}}^2 = 1/3$ of about 11 km established in Ref. [28] (Fig. 5) using the EoS that yields maximally compact stars (corresponding to CSS with $p_{\text{trans}} = 0$ and $c_{\text{QM}}^2 = 1/3$) obeying $M_{\text{max}} > 2M_{\odot}$. If a $1.4M_{\odot}$ star were observed to have radius below the minimum value, one would have to conclude that either it is not a hybrid star or that $c_{\text{QM}}^2 > 1/3$.

The dashed line shows how the excluded region would grow if a star of mass $2.1M_{\odot}$ were to be observed. This would increase the minimum radius to about 12.7 (BHF) or 13 km (DBHF).

III. THE BHF AND DBHF EOS OF NUCLEAR MATTER

We now discuss in more detail the nuclear matter equations of state that we use in this work. We adopt the BHF scheme, in which the only input needed is the realistic free nucleon-nucleon (NN) interaction V in the Brueckner-Bethe-Goldstone (BBG) equation for the reaction matrix G ,

$$G[\rho; \omega] = V + \sum_{k_a k_b} V \frac{|k_a k_b\rangle Q \langle k_a k_b|}{\omega - e(k_a) - e(k_b)} G[\rho; \omega], \quad (3)$$

where ρ is the nucleon number density, and ω the starting energy. The propagation of intermediate baryon pairs is determined by the single-particle energy $e(k; \rho) = \frac{k^2}{2m} + U(k; \rho)$, and the Pauli operator Q . Because of the oc-

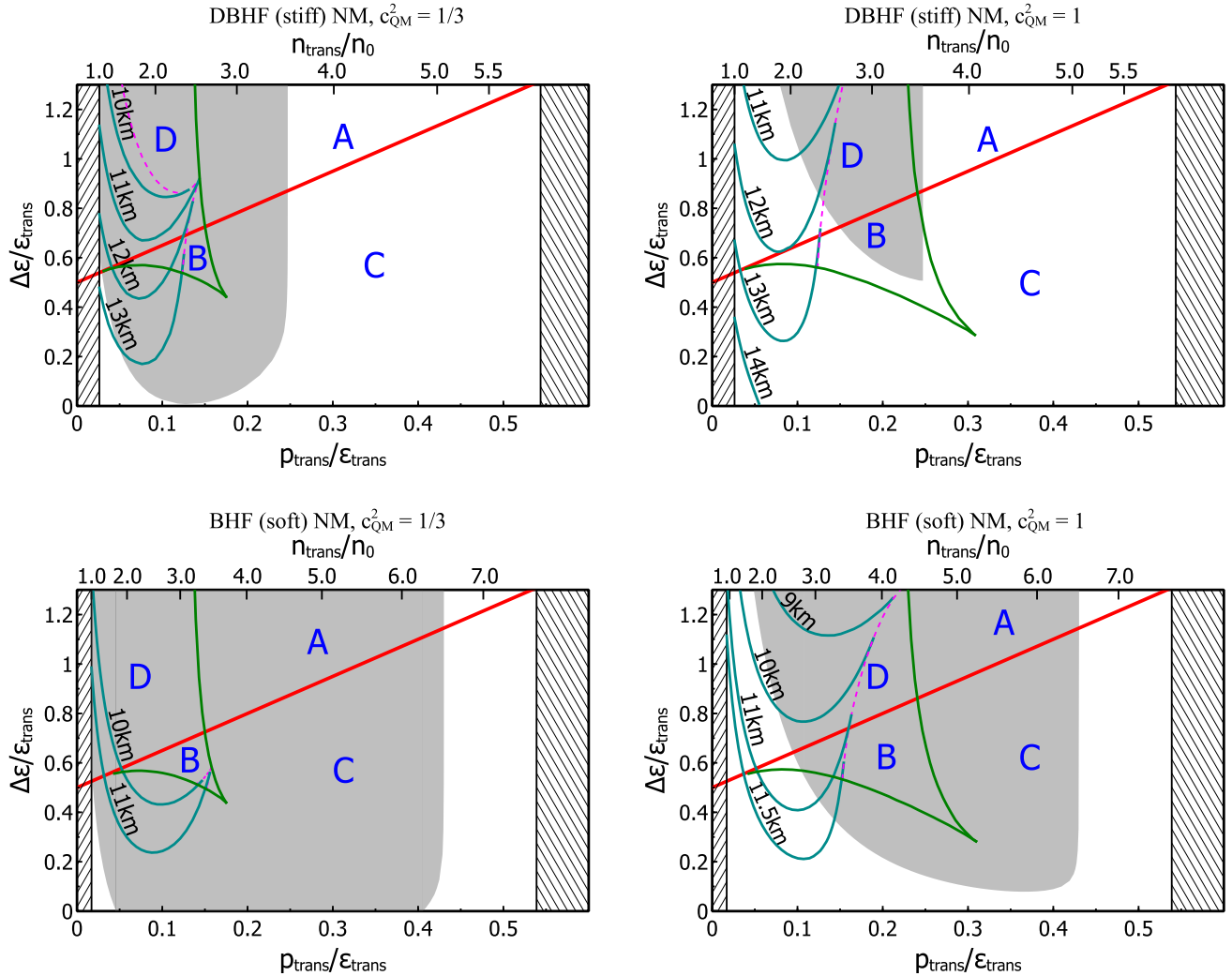


FIG. 4: (Color online). Contour plots similar to Fig. 3 showing the radius of a hybrid star of mass $M = 1.4M_{\odot}$ as a function of the CSS parameters. Such stars only exist in a limited region of the space of EoSs [delimited by dashed (magenta) lines]. The grey shaded region is excluded by the observational constraint $M_{\text{max}} > 2M_{\odot}$. For a magnified version of the low-transition-pressure region for $c_{\text{QM}}^2 = 1/3$, see Fig. 5.

cence of G in the single-particle potential $U(k;\rho) = \text{Re} \sum_{k' \leq k_F} \langle kk' | G[\rho; e(k) + e(k')] | kk' \rangle_a$, where the subscript “ a ” indicates antisymmetrization of the matrix element, the BBG equation (Eq. (3)) has to be solved in a self-consistent manner for several momenta of the particles involved, at the considered densities.

In the nonrelativistic BHF approximation the energy per nucleon is given by [29]

$$\frac{E}{A} = \frac{3}{5} \frac{k_F^2}{2m} + \frac{1}{2\rho} \sum_{k,k' \leq k_F} \langle kk' | G[\rho; e(k) + e(k')] | kk' \rangle_a. \quad (4)$$

The nuclear EoS can be calculated with good accuracy in the Brueckner two hole-line approximation with the continuous choice for the single-particle potential, and the results in this scheme are quite close to the calculations which include also the three hole-line contribution [30–32]. The dependence on

the NN interaction, also within other many-body approaches, has been systematically investigated in Ref. [33].

It is well known that, in order to reproduce the correct saturation point of symmetric nuclear matter, we must introduce nuclear three-body forces (TBFs). In our approach the TBF is reduced to a density-dependent two-body force by averaging over the position of the third particle, assuming that the probability of having two particles at a given distance is reduced according to the two-body correlation function [34, 35].

In this work we use the Argonne v₁₈ NN potential [36], and the so-called Urbana model for TBFs, which consists of an attractive term due to two-pion exchange with excitation of an intermediate Δ resonance, and a repulsive phenomenological central term [37, 38]. Those TBFs produce a shift of about +1 MeV in energy and -0.01 fm^{-3} in density. This adjustment is obtained by tuning the two parameters contained in the TBFs, and was performed to get an optimal saturation point

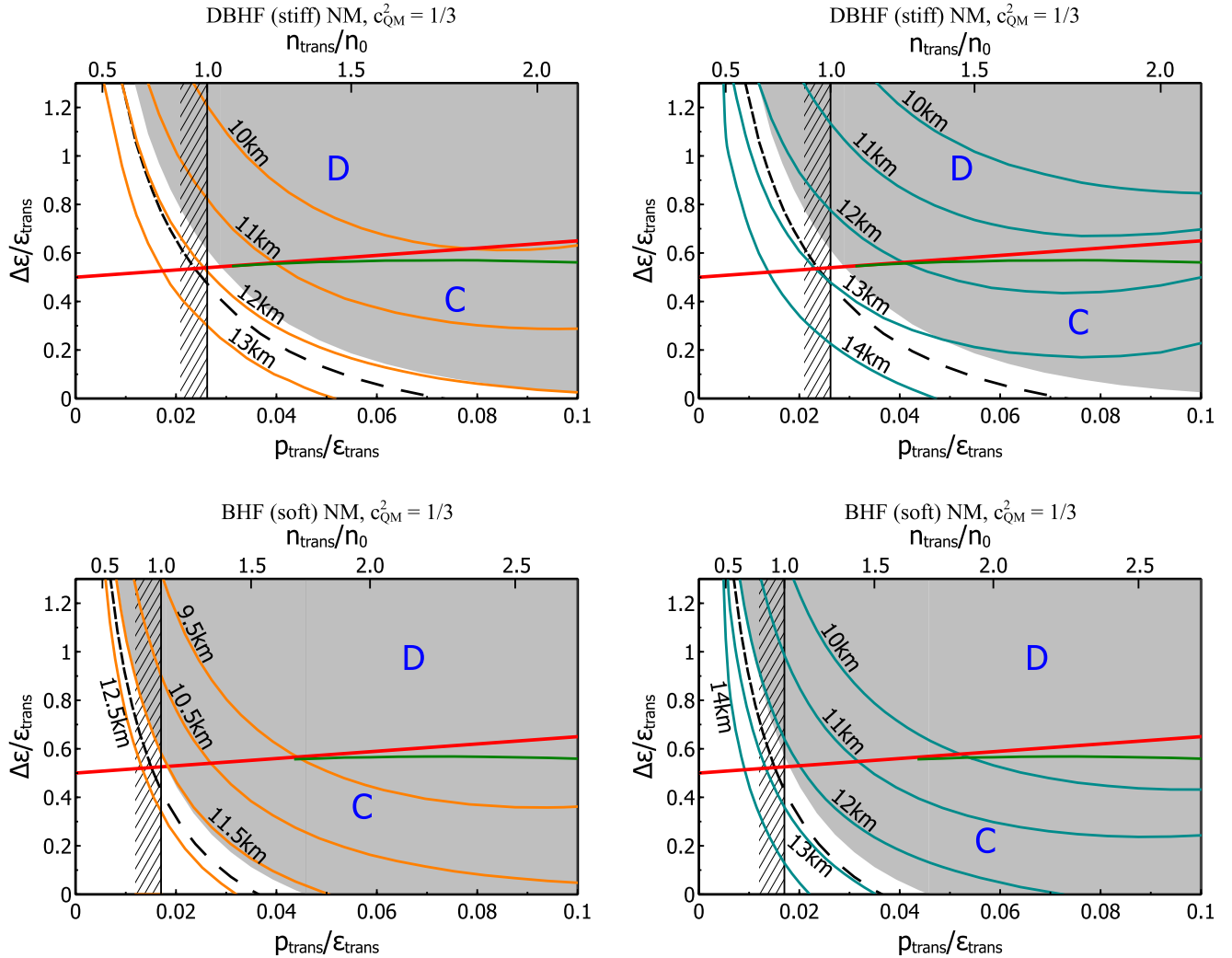


FIG. 5: (Color online). Magnified version of the $c_{QM}^2 = 1/3$ plots in Figs. 3–4. In the two left panels, the contours are for the radius of the maximum-mass star, which is typically the smallest star for the given EoS. In the two right panels, the contours are for $R_{1.4}$, the radius of a $1.4 M_{\odot}$ star. The region under and to the left of the hatched bar is probably unphysical because $n_{trans} < n_0$, and it was excluded (hatched band) in earlier figures. The grey shaded region is excluded by the observational constraint $M_{max} > 2 M_{\odot}$. The dashed line shows how that region would grow if a $2.1 M_{\odot}$ star were observed.

[34, 35]. At present the theoretical status of microscopically derived TBFs is still quite rudimentary; however a tentative approach has been proposed using the same meson-exchange parameters as the underlying NN potential [39, 40].

Along with the nonrelativistic BHF EoS we consider its relativistic counterpart, the DBHF scheme [24] where the Bonn-A potential is used for the nucleon-nucleon interaction. In the low density region ($\rho < 0.3 \text{ fm}^{-3}$), the BHF (including TBF) and DBHF equations of state are very similar, whereas at higher densities the DBHF is slightly stiffer. The discrepancy between the nonrelativistic and relativistic calculation can be easily understood by recalling that the DBHF treatment is equivalent to introducing in the nonrelativistic BHF the TBF corresponding to the excitation of a nucleon-antinucleon pair, the so-called Z-diagram [41], which is repulsive at all densities. In the BHF treatment with Urbana TBF, both attractive

and repulsive TBF are introduced and therefore a softer EoS is expected. We report in Table I the main properties of both EoSs.

In this work we perform all calculations for both the BHF and DBHF equations of state for hadronic matter. This provides a reasonable range of possible hadronic EoSs, and allows us to gauge the sensitivity of our results to this source of uncertainty, although even DBHF is not as stiff as an ultrastiff hadronic EoS such as DD2-EV [26] (see Sec. II B).

We do not include the effects of hyperons because these are unknown, and including them would not increase the physical accuracy of our results. Calculating a hyperonic EoS requires knowledge of hyperon interactions with other baryons, and there is little data on hyperon-nucleon interactions [42] and none on hyperon-hyperon interactions or three-body interactions. There have been various conjectures about the hyperon

interaction [43–46] and how to include it in BHF [44, 47, 48] and DBHF [49] but there is no consensus on the correct result.

IV. QUARK MATTER VIA THE FIELD CORRELATOR METHOD

A. The FCM EoS

The approach based on the FCM provides a natural treatment of the dynamics of confinement in terms of the color electric (D^E and D_1^E) and color magnetic (D^H and D_1^H) Gaussian correlators, the former being directly related to confinement, so that its vanishing above the critical temperature implies deconfinement [50]. The extension of the FCM to finite temperature T at chemical potential $\mu_q = 0$ gives analytical results in reasonable agreement with lattice data, giving us some confidence that it correctly describes the deconfinement phase transition [51, 52]. In order to derive an EoS of the quark-gluon matter in the range of baryon density typical of the neutron star interiors, we have to extend the FCM to nonzero chemical potential [51, 52]. In this case, the quark pressure for a single flavor is simply given by

$$P_q/T^4 = \frac{1}{\pi^2} \left[\phi_v \left(\frac{\mu_q - V_1/2}{T} \right) + \phi_v \left(-\frac{\mu_q + V_1/2}{T} \right) \right] \quad (5)$$

where

$$\phi_v(a) = \int_0^\infty du \left(u^4 / \sqrt{u^2 + v^2} \right) \left(\exp \left[\sqrt{u^2 + v^2} - a \right] + 1 \right)^{-1} \quad (6)$$

with $v = m_q/T$, and V_1 is the large distance static $\bar{q}q$ potential whose value at zero chemical potential and temperature is $V_1(T = \mu_B = 0) = 0.8$ to 0.9 GeV [53, 54]. The gluon contribution to the pressure is

$$P_g/T^4 = \frac{8}{3\pi^2} \int_0^\infty d\chi \chi^3 \frac{1}{\exp \left(\chi + \frac{9V_1}{8T} \right) - 1} \quad (7)$$

and the total pressure is

$$P_{qg} = \sum_{j=u,d,s} P_q^j + P_g - \frac{(11 - \frac{2}{3}N_f)}{32} \frac{G_2}{2} \quad (8)$$

where P_q^j and P_g are given in Eqs. (5) and (7), and N_f is the number of flavors. The last term in Eq. (8) corresponds to the difference of the vacuum energy density in the two phases, G_2 being the gluon condensate whose numerical value, determined by the QCD sum rules at zero temperature and chemical potential, is known with large uncertainty, $G_2 = 0.012 \pm 0.006$ GeV 4 . At finite temperature and vanishing baryon density, a comparison with the recent available lattice calculations provides clear indications about the specific values of these two parameters, and in particular their values at the critical temperature T_c . Some lattice simulations suggest no dependence of V_1 on μ_B , at least for very small μ_B , while different analyses suggest a linear decreasing of G_2 with the

baryon density ρ_B [55], in nuclear matter. However, for simplicity, in the following we treat both V_1 and G_2 as numerical parameters with no dependence on μ_B .

B. The FCM EoS and the CSS parametrization

The CSS parametrization will be applicable to the FCM EoS if the speed of sound in the FCM EoS depends only weakly on the density or pressure. In Fig. 6 we show that this is indeed the case. The upper panel shows the speed of sound vs. pressure in the FCM quark matter EoS for different values of the FCM parameters, displayed in the lower panel. We see that the speed of sound varies by less than 5% over the considered range of pressures along each curve, and lies in the interval $0.28 < c_{QM}^2 < 1/3$. The value of c_{QM}^2 shows a weak dependence on V_1 and extremely weak dependence on G_2 , which appears as an additive constant in the quark matter EoS according to Eq. (8). The transition pressure is more sensitive to the FCM parameters, increasing rapidly with V_1 and with G_2 . The energy density at a given pressure increases slightly with an increase in V_1 or G_2 .

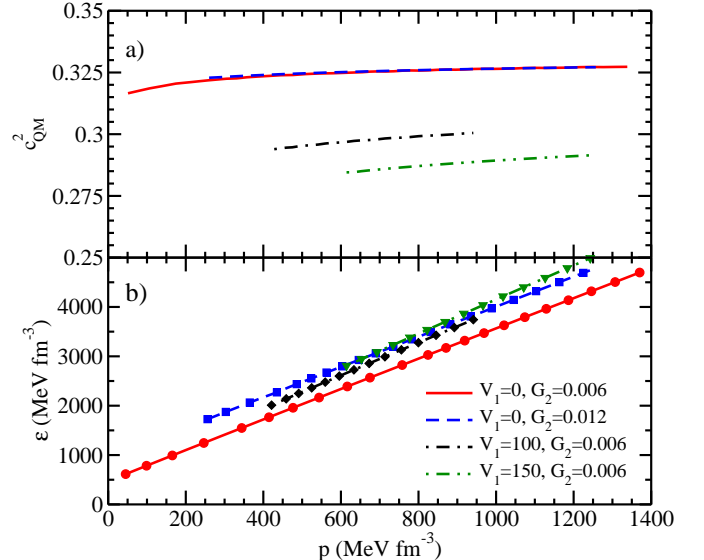


FIG. 6: (Color online). The squared speed of sound c_{QM}^2 [panel (a)] is displayed vs quark matter pressure for several values of V_1 (in MeV) and G_2 (in GeV 4). In panel (b), the FCM energy density is represented by full symbols, whereas the full lines denote the CSS parametrization given by Eq. (1).

To illustrate how well the CSS parametrization fits the FCM EoS, we show in the lower panel of Fig. 6 that, for the same FCM parameter choices, we can always find suitable values of the CSS parameters which fit the FCM calculation extremely well. This means that there exists a well-defined mapping between the FCM parameters (V_1, G_2) and the CSS parameters ($p_{trans}/\epsilon_{trans}, \Delta\epsilon/\epsilon_{trans}, c_{QM}^2$). Note that the mapping depends on the EoS of the hadronic matter.

The mapping is displayed in Fig. 7, which shows the region

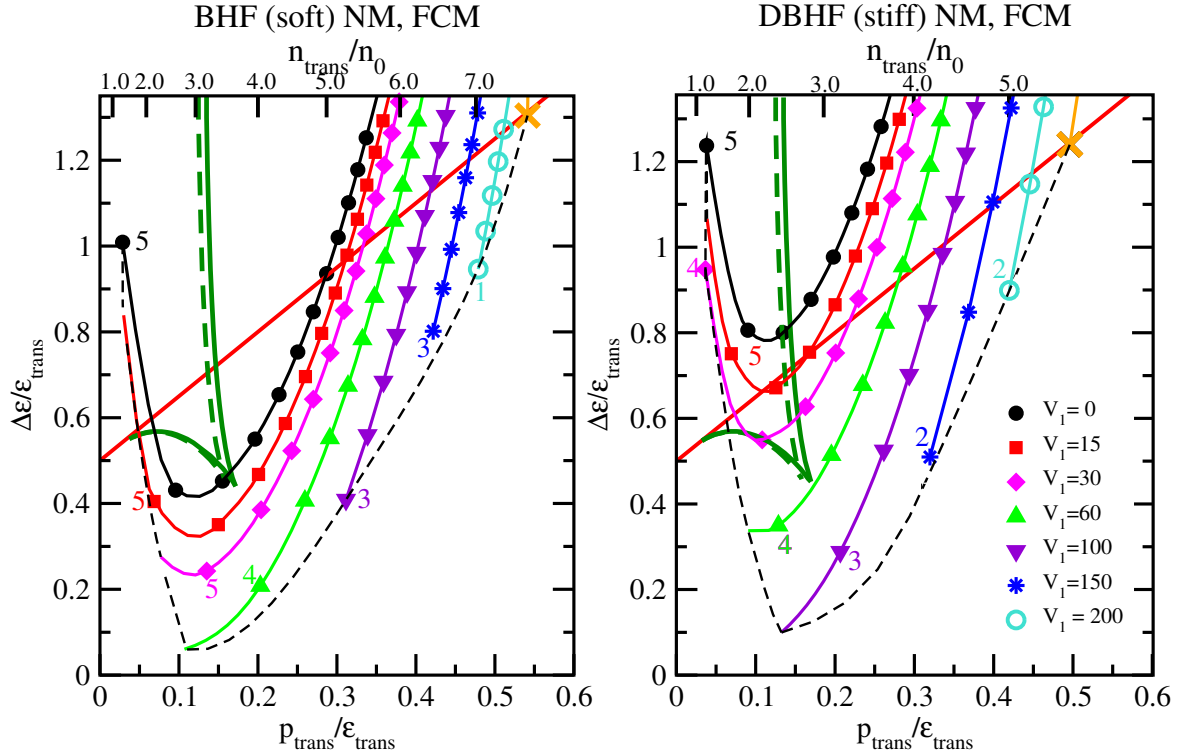


FIG. 7: (Color online). The mapping of the FCM quark matter model onto the CSS parametrization. Results are obtained using the BHF (left panel) and DBHF (right panel) nuclear matter EoS. The undecorated curves are the phase boundaries for the occurrence of connected and disconnected hybrid branches (compare Figs. 1 and 2). The thin dashed (black) line and the solid (black) line studded with circles delimit the region yielded by the FCM model. Within that region, lines decorated with symbols give CSS parameter values for FCM quark matter as G_2 is varied at constant V_1 (given in MeV). The (orange) cross denotes the EoS with the highest p_{trans} , which gives the heaviest FCM hybrid star. See the text for details.

of the CSS parameter space where FCM equations of state are found. As in the phase diagrams in Sec. II, we show the plane whose coordinates are the CSS parameters $\Delta\epsilon/\epsilon_{\text{trans}}$ and $p_{\text{trans}}/\epsilon_{\text{trans}}$. For the hadronic EoS we use BHF (left panel) and DBHF (right panel). The lines without points represent the phase boundaries, as for the figures in Sec. II, for connected and disconnected branches. Whether a given FCM EoS yields stable hybrid stars depends on which of those phase regions (see Fig. 1) it is in. The solid (green) phase boundary with a cusp at $p_{\text{trans}}/\epsilon_{\text{trans}} \approx 0.17$ delimits the region with a disconnected branch for $c_{\text{QM}}^2 = 1/3$, while the nearby dashed (green) line is for $c_{\text{QM}}^2 = 0.28$, so these span the range of c_{QM}^2 relevant for the FCM, as discussed in Fig. 6. It is evident that the dependence on c_{QM}^2 is tiny and negligible for practical purposes.

The thin dashed (black) line and the solid (black) line studded

with circles delimit the equations of state yielded by the FCM calculation. Within that region, the lines studded with points show the CSS parametrization of the FCM quark matter EoS, where along each line we keep V_1 constant and vary G_2 . Above that region, which corresponds to negative values of V_1 , the EoS cannot reproduce the $2M_\odot$ limit, and in this sense is unphysical (Fig. 8). Below that region, there would be no transition from hadronic to quark matter, as explained below.

In Fig. 7, V_1 varies from 0 up to the maximum value at which hybrid star configurations occur, which is indicated by an (orange) cross. For the BHF case that value is $V_1 = 240$ MeV, $G_2 = 0.0024 \text{ GeV}^4$ and for the DBHF case it is $V_1 = 255$ MeV, $G_2 = 0.0019 \text{ GeV}^4$. Along each FCM curve in Fig. 7 the parameter G_2 starts at the minimum value at which

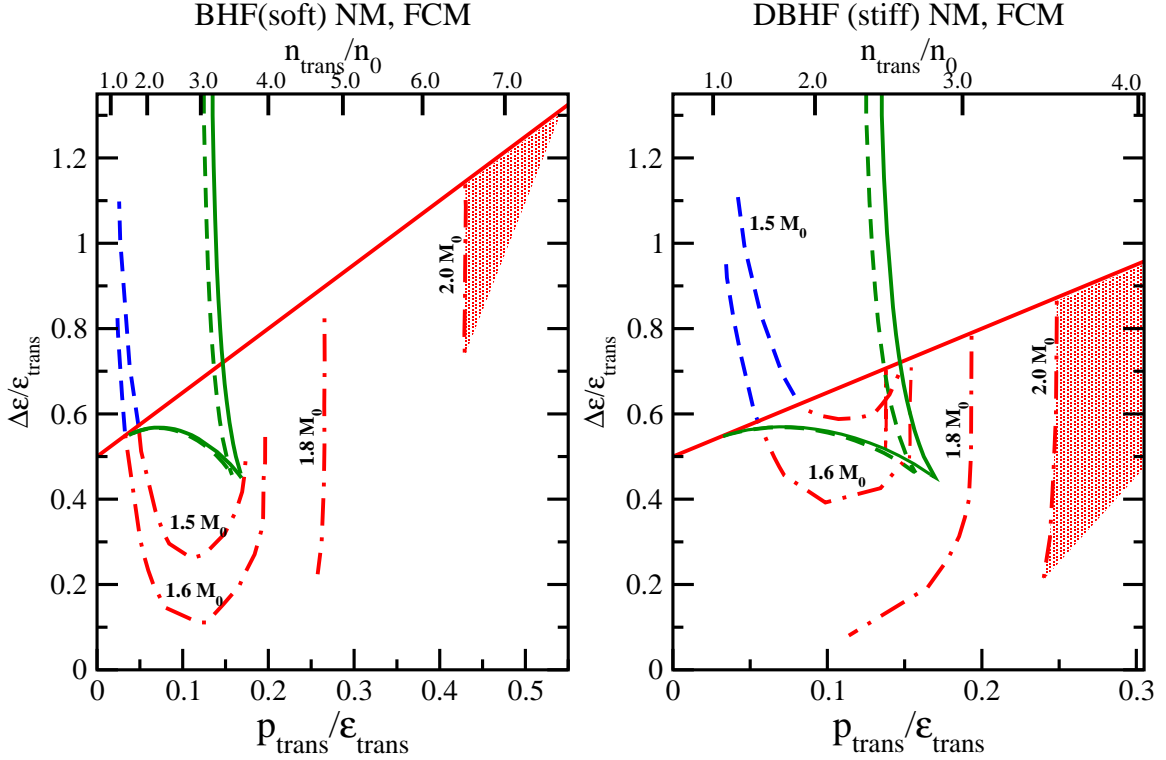


FIG. 8: (Color online). Contour plots, analogous to Fig. 2, showing the maximum mass of hybrid stars with FCM quark matter cores, given in terms of the corresponding CSS parameter values rather than the original FCM parameter values. As in Fig. 7, solid lines are phase boundaries (compare Figs. 1 and 2). The shaded sectors indicate the parameter regions accessible by the FCM and with $M_{\max} > 2M_{\odot}$. In each panel the lower border of the shaded region meets the phase boundary (red line) at the point with highest value of V_1 reported in Fig. 7 as an orange cross. Note the different scales on the x axis for the two panels.

there is a phase transition from hadronic to FCM quark matter; at lower G_2 the quark and the hadronic pressures $p(\mu)$ do not cross at any μ . On each curve one point is labeled with its value of $G_2/(10^{-3} \text{ GeV}^4)$, and subsequent points are at intervals where G_2 increases in increments of 1 in the same units.

We observe that along each line of constant V_1 , $p_{\text{trans}}/\epsilon_{\text{trans}}$ grows with G_2 . This can be explained by recalling the linear dependence of the quark pressure on G_2 in Eq. (8), so that, at fixed chemical potential, an increase of G_2 lowers the quark pressure, making quark matter less favorable, and shifting the transition point to higher chemical potential or pressure. This was already discussed in Ref. [56] for BHF nuclear matter, and is equally applicable to DBHF nuclear matter. Obviously if G_2 becomes too small, the phase transition takes place in a region of low densities where finite nuclei are present, and the homogeneous nuclear matter approach becomes invalid.

The qualitative behavior of the curves of constant V_1 can be understood in terms of the Maxwell construction between the purely hadronic phase and the quark phase. The fact that $\Delta\epsilon/\epsilon_{\text{trans}}$ goes through a minimum (which is always at $p_{\text{trans}}/\epsilon_{\text{trans}} \approx 0.1$) as G_2 is increased at constant V_1 can be understood from Fig. 2 of Ref. [56], which shows pressure p as a function of baryon density n and the location of the hadron (BHF EoS) to quark (FCM EoS) transition when G_2 is varied. The hadronic EoS is strongly curved, especially at low pressure, while the FCM EoS is closer to a straight line. Consequently, the baryon density difference between the two phases at a given pressure has a minimum at densities around $2n_0$, which corresponds to $p_{\text{trans}}/\epsilon_{\text{trans}} \approx 0.1$. As G_2 increases, the transition pressure rises, scanning through this minimum. It follows that the energy density difference also goes through a minimum, because $\epsilon = \mu n - p$, and p and μ are continuous at

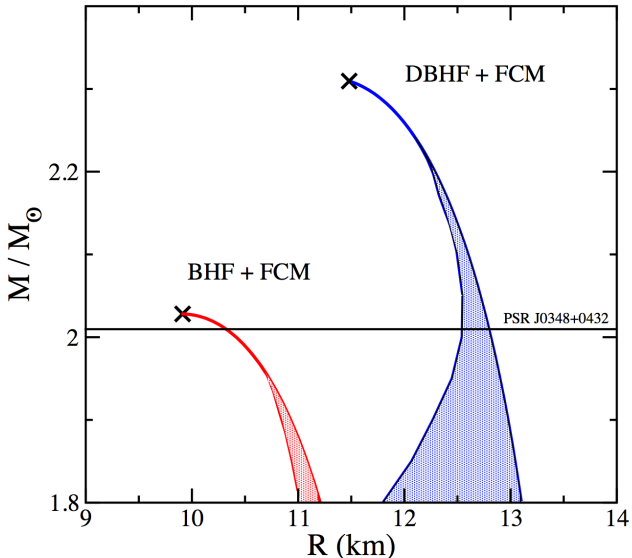


FIG. 9: (Color online). Shaded areas show range of radii of stars with a given maximum mass when varying FCM parameters. The thick dashed lines indicate the purely hadronic mass-radius configurations. The crosses at the top of the shaded regions correspond to the maximal configuration indicated by the same symbol in Fig. 7. The observational constraint [23] on the star mass is indicated by a horizontal line.

the transition, so $\Delta\epsilon = \mu\Delta n$. The DBHF hadronic EoS is very similar to BHF at low pressure, so the curves have their minima at the same value of $p_{\text{trans}}/\epsilon_{\text{trans}}$ in both panels of Fig. 7.

We also see in Fig. 7 that an increase of V_1 moves the curves slightly downward and to the right. This is expected since V_1 is a measure of the interparticle strength, and is inversely proportional to the pressure of the system, so that the pressure decreases as V_1 is increased at fixed μ , and, as already discussed for the parameter G_2 , a decrease of the quark pressure raises p_{trans} . The role of V_1 and G_2 in the quark EoS discussed so far, provides in the same way a qualitative understanding of c_{QM}^2 in panel (a) in Fig. 6, although, as already noticed, the effect in Fig. 7 of the change in c_{QM}^2 is negligible.

C. Expected properties of mass-radius curves

By comparing Fig. 7 with Fig. 1 we can see that when combining FCM quark matter with BHF (soft) nuclear matter, the physically allowed range of FCM parameter values yields EoSs that are mostly in regions C and A, where there is no disconnected hybrid branch. At the lowest transition densities the FCM EoS can achieve a large enough energy density discontinuity to yield a disconnected branch (region D).

For the DBHF (stiff) nuclear EoS there is a wider range of values of V_1 and G_2 that give disconnected branches, and

some of them give simultaneous connected and disconnected branches. This difference can be understood in terms of the stiffness of the EoSs. A change from a soft hadronic EoS (BHF) to a stiff one (DBHF) produces a steeper growth of the hadronic pressure as a function of the baryon density. Referring again to Fig. 2 of Ref. [56], this pulls the DBHF $p(n)$ curve further away from the FCM curve, giving a larger difference in baryon density at a given pressure, and hence, as noted above, a larger $\Delta\epsilon$. This is why the curves for DBHF+FCM (right panel of Fig. 7) are shifted upwards along the $\Delta\epsilon/\epsilon_{\text{trans}}$ axis compared to the BHF+FCM curves (left panel of Fig. 7).

We can calculate the maximum mass of a hybrid star containing a FCM core as a function of the FCM parameters, and then use the mapping described above to obtain the CSS parameter values for each FCM EoS, producing a contour plot of maximum mass (Fig. 8) for BHF (left panel) and DBHF (right panel) hadronic EoS. Given that the CSS parametrization is a fairly accurate representation of the FCM EoS, one would expect this to be very similar to the corresponding plot for CSS itself with $c_{\text{QM}}^2 = 1/3$ (Fig. 2), and this is indeed the case. The contours in Fig. 8 are restricted to the region corresponding to physically allowed FCM parameter values, so they end at the edges of that region.

The triangular shaded area at the edge of each panel shows the region of the parameter space that is accessible by the FCM and is consistent with the measurement of a $2M_\odot$, by having hybrid stars of maximum mass greater than $2M_\odot$. The (orange) cross in each panel of Fig. 7 is at the high-transition-pressure corner of that triangular area. The heaviest BHF+FCM hybrid star has a mass of $2.03M_\odot$, and the heaviest DBHF+FCM hybrid star has a mass of $2.31M_\odot$.

As noted in Sec. II B, the hybrid stars in this physically allowed and FCM-compatible region of the phase diagram lie on a very tiny connected branch, covering a very small range of central pressures and masses and radii, and would therefore occur only rarely in nature. These stars have very small quark matter cores (see Ref. [1], Figs. 5–6), and their mass and radius are very similar to those of the heaviest purely hadronic star, but there could be other clear signatures of the presence of the quark matter core, such as different cooling behavior.

The CSS parametrization has another region where heavy hybrid stars occur, at low transition pressure (see Fig. 2), but the FCM does not predict that the quark matter EoS could be in that region.

To characterize the radius of FCM hybrid stars we cannot construct contour plots like Fig. 4 because, as we have just seen, the FCM predicts that only hybrid stars with mass very close to the maximum mass are allowed. There are no FCM hybrid stars with mass around $1.4M_\odot$. Instead, in Fig. 9 we show the range of radii of stars with a given maximum mass when varying FCM parameters, for our two different hadronic EoSs. The right-hand edge of each shaded region traces out the mass-radius relation for hadronic stars with the corresponding hadronic EoS. The FCM hybrid stars form very small connected branches which connect to the nuclear matter where the central pressure reaches the transition pressure (see Sec. II B), so the hybrid stars do not deviate very far from the hadronic mass-radius curve. Hence the shaded regions in

Fig. 9 are narrow, especially in the observationally allowed ($M_{\max} > 2M_{\odot}$) region, which perfectly matches the prediction of CSS parametrization on the maximum-mass star radius in the high-transition-pressure region (see the left panels of Fig. 3). For BHF (soft) nuclear matter, the hadronic stars, and hence the hybrid stars, are smaller because the nuclear mantle is more compressed by the self gravitation of the star.

V. CONCLUSIONS

We have shown how observational constraints on the mass and radius of hybrid stars can be expressed as constraints on the parameters of the CSS parametrization of the high-density EoS, which, in the space of possible models of quark matter, is a reasonably model-independent parametrization. Of course, physical predictions from CSS depend on the hadronic EoS with which it is combined. The CSS parametrization assumes a sharp transition from nuclear matter to a high-density phase such as quark matter, and that the speed of sound in that phase is independent of the pressure. We found that the observation of a $2M_{\odot}$ star constrains the CSS parameters significantly [1, 18].

If, as predicted by many physical models of quark matter, $c_{\text{QM}}^2 \lesssim 1/3$, then for typical models of hadronic matter such as BHF or DBHF there are two possible scenarios (we discuss ultrastiff hadronic EoSs below).

First, there is a low-transition-pressure scenario, where the transition to the high-density phase occurs at $n_{\text{trans}} \lesssim 2n_0$ (the unshaded region on the left side of the two left panels of Figs. 2–4). In this scenario, the hybrid branch of the mass-radius relation will be connected to the nuclear branch. In the $c_{\text{QM}}^2 \lesssim 1/3$ and low-transition-pressure scenario there are strong constraints on the radius of the star, as shown in Fig. 5. The radius of the maximum-mass star (which is typically the smallest possible star) must be greater than about 11.5 km, and the radius of a $1.4M_{\odot}$ star must be greater than about 12.2 km [28]. For a stiffer hadronic EoS, these minima are raised by about 0.15 to 0.3 km. If a neutron star of mass $2.1M_{\odot}$ were observed then this constraint would tighten, increasing the minimum radius to about 12.1 km. If a star smaller than the minimum radius were observed, we would have to conclude that either the transition is outside the low-density regime or $c_{\text{QM}}^2 > 1/3$. Conversely, if theoretical considerations established that c_{QM}^2 is smaller than $1/3$, the minimum radius would become larger [18].

Secondly, there is a high-transition-pressure scenario (the white region on the right side of the left panels of Figs. 2–4). This tends to give a very small branch of hybrid stars with tiny quark matter cores, occurring in a narrow range of central pressures just above the transition pressure. This is why the mass and radius contours become almost vertical in this region: the hybrid star has almost the same mass and radius as the heaviest purely hadronic star (the one where the central pressure is p_{trans}), and so the properties of these hybrid stars depend on the hadronic EoS (see Fig. 9) via $p_{\text{trans}}/\varepsilon_{\text{trans}}$ but not on quark matter properties such as $\Delta\varepsilon$ or c_{QM}^2 .

If the hadronic matter is extremely stiff (e.g. DD2-EV [26])

or the quark matter has c_{QM}^2 larger than $1/3$ then a larger region of the CSS parameter space becomes allowed. The right panels of Figs. 2–4 show the extreme case where $c_{\text{QM}}^2 = 1$. In this case the minimum possible radius is 9.0 km.

Disconnected hybrid branches are of special interest, because they give a characteristic signature in mass-radius measurements. For both the hadronic EoSs that we study, disconnected hybrid star branches are excluded by the $M_{\max} > 2M_{\odot}$ constraint for $c_{\text{QM}}^2 \leq 1/3$, and even for larger c_{QM}^2 they only arise if the hadronic matter EoS is stiff. Explorations of the ultrastiff hadronic DD2-EV EoS indicate that disconnected hybrid star branches can occur at moderate c_{QM}^2 , and it would be interesting to include this EoS in a future study.

Our work is intended to motivate the use of the CSS parametrization as a framework in which the implications of observations of neutron stars for the high-density EoS can be expressed and discussed in a way that is reasonably independent of the modeling of the EoS of the high-density phase (quark matter in our case) [4, 26].

As an application to a specific model, we performed calculations for the FCM quark matter EoS. We showed that the FCM equation of state can be accurately represented by the CSS parametrization, and we displayed the mapping between the FCM and CSS parameters. We found that FCM quark matter has a speed of sound in a narrow range around $c_{\text{QM}}^2 = 0.3$, and the FCM family of EoSs covers a limited region of the space of all possible EoSs (Fig. 7). Once the observational constraint $M_{\max} > 2M_{\odot}$ is taken into account, the allowed region in the parameter space is drastically reduced to the shaded areas of Fig. 8. This corresponds to the high-transition-pressure scenario, with a small connected branch of hybrid stars with tiny quark matter cores. Such stars would be hard to distinguish from hadronic stars via mass and radius measurements, but the quark matter core could be detectable via other signatures, such as cooling behavior. These hybrid stars have central densities larger than $6.5n_0$ in the BHF case, and $3.5n_0$ in the DBHF case (Fig. 8) which means that, according to Refs. [43, 44, 46, 49], hyperons could play an important role in the BHF case, and they cannot be ruled out even in the relativistic DBHF case. As discussed in Sec. III, we ignored hyperons because we are already using two different hadronic EoSs, one stiff and one soft, to estimate the sensitivity of our results to the hadronic EoS, and the effect of hyperons remains unknown. In the future we hope that more experimental data will constrain the high-density hadronic EoS, including the hyperonic contribution.

VI. ACKNOWLEDGMENTS

This material is based upon work supported by the U.S. Department of Energy (DOE), Office of Science, Office of Nuclear Physics under Award No. DE-FG02-05ER41375, and by the DOE Topical Collaboration “Neutrinos and Nucleosynthesis in Hot and Dense Matter” Grant No. de-sc0004955. Partial support comes from “NewCompStar,” COST Grant No. MP1304. We thank J. Lattimer, F. Weber, D. Blaschke, and M. Prakash for helpful discussions.

[1] M. G. Alford, S. Han, and M. Prakash, *Generic conditions for stable hybrid stars*, Phys. Rev. D **88** (Oct, 2013) 083013.

[2] J. Zdunik and P. Haensel, *Maximum mass of neutron stars and strange neutron-star cores*, Astron.Astrophys. **551** (2013) A61, [[arXiv:1211.1231](https://arxiv.org/abs/1211.1231)].

[3] N. Chamel, A. Fantina, J. Pearson, and S. Goriely, *Maximum mass of neutron stars with exotic cores*, Astron.Astrophys. **553** (2013) A22, [[arXiv:1205.0983](https://arxiv.org/abs/1205.0983)].

[4] A. Ayriyan, D. E. Alvarez-Castillo, D. Blaschke, H. Grigorian, and M. Sokolowski, *New Bayesian analysis of hybrid EoS constraints with mass-radius data for compact stars*, Phys. Part. Nucl. **46** (2015), no. 5 854–857, [[arXiv:1412.8226](https://arxiv.org/abs/1412.8226)].

[5] R. Schaeffer, L. Zdunik, and P. Haensel, *Phase transitions in stellar cores. I - Equilibrium configurations*, Astron. Astrophys. **126** (Sept., 1983) 121–145.

[6] M. Alford, K. Rajagopal, S. Reddy, and F. Wilczek, *Minimal color-flavor-locked nuclear interface*, Phys. Rev. D **64** (Sep, 2001) 074017.

[7] L. F. Palhares and E. S. Fraga, *Droplets in the cold and dense linear sigma model with quarks*, Phys. Rev. D **82** (Dec, 2010) 125018.

[8] M. B. Pinto, V. Koch, and J. Randrup, *Surface tension of quark matter in a geometrical approach*, Phys. Rev. C **86** (Aug, 2012) 025203.

[9] J. Macher and J. Schaffner-Bielich, *Phase transitions in compact stars*, Eur.J.Phys. **26** (2005) 341–360, [[astro-ph/0411295](https://arxiv.org/abs/astro-ph/0411295)].

[10] K. Masuda, T. Hatsuda, and T. Takatsuka, *Hadron–quark crossover and massive hybrid stars*, PTEP **2013** (2013), no. 7 073D01, [[arXiv:1212.6803](https://arxiv.org/abs/1212.6803)].

[11] D. E. Alvarez-Castillo, S. Benić, D. Blaschke, and R. Łastowiecki, *Crossover transition to quark matter in heavy hybrid stars*, Acta Phys.Polon.Supp. **7** (2014), no. 1 203–208, [[arXiv:1311.5112](https://arxiv.org/abs/1311.5112)].

[12] B. K. Agrawal, *Equations of state and stability of color-superconducting quark matter cores in hybrid stars*, Phys. Rev. D **81** (Jan, 2010) 023009.

[13] L. Bonanno and A. Sedrakian, *Composition and stability of hybrid stars with hyperons and quark color-superconductivity*, Astron.Astrophys. **539** (2012) A16, [[arXiv:1108.0559](https://arxiv.org/abs/1108.0559)].

[14] R. Łastowiecki, D. Blaschke, H. Grigorian, and S. Typel, *Strangeness in the cores of neutron stars*, Acta Phys.Polon.Supp. **5** (2012) 535–540, [[arXiv:1112.6430](https://arxiv.org/abs/1112.6430)].

[15] A. Kurkela, P. Romatschke, A. Vuorinen, and B. Wu, *Looking inside neutron stars: Microscopic calculations confront observations*, [arXiv:1006.4062](https://arxiv.org/abs/1006.4062).

[16] A. Kurkela, P. Romatschke, and A. Vuorinen, *Cold quark matter*, Phys. Rev. D **81** (May, 2010) 105021.

[17] M. Alford, M. Braby, M. Paris, and S. Reddy, *Hybrid stars that masquerade as neutron stars*, Astrophys.J. **629** (2005) 969–978, [[nucl-th/0411016](https://arxiv.org/abs/nucl-th/0411016)].

[18] P. Bedaque and A. W. Steiner, *Sound velocity bound and neutron stars*, Phys. Rev. Lett. **114** (Jan, 2015) 031103.

[19] T. Kojo, P. D. Powell, Y. Song, and G. Baym, *Phenomenological qcd equation of state for massive neutron stars*, Phys. Rev. D **91** (Feb, 2015) 045003.

[20] S. Benic, *Heavy hybrid stars from multi-quark interactions*, Eur.Phys.J. **A50** (2014) 111, [[arXiv:1401.5380](https://arxiv.org/abs/1401.5380)].

[21] Z. F. Seidov, *The Stability of a Star with a Phase Change in General Relativity Theory*, Sov. Astron. **15** (Oct., 1971) 347.

[22] L. Lindblom, *Phase transitions and the mass-radius curves of relativistic stars*, Phys. Rev. D **58** (Jun, 1998) 024008.

[23] J. Antoniadis, P. Freire, N. Wex, T. Tauris, R. Lynch, and et al., *A Massive Pulsar in a Compact Relativistic Binary*, Science **340** (2013) 1233232, [[arXiv:1304.6875](https://arxiv.org/abs/1304.6875)].

[24] T. Gross-Boelting, C. Fuchs, and A. Faessler, *Covariant representations of the relativistic Brückner T matrix and the nuclear matter problem*, Nucl.Phys. **A648** (1999) 105–137, [[nucl-th/9810071](https://arxiv.org/abs/nucl-th/9810071)].

[25] G. Taranto, M. Baldo, and G. F. Burgio, *Selecting microscopic equations of state*, Phys. Rev. C **87** (Apr, 2013) 045803.

[26] S. Benic, D. Blaschke, D. E. Alvarez-Castillo, T. Fischer, and S. Typel, *A new quark-hadron hybrid equation of state for astrophysics - I. High-mass twin compact stars*, Astron. Astrophys. **577** (2015) A40, [[arXiv:1411.2856](https://arxiv.org/abs/1411.2856)].

[27] A. V. Yudin, T. L. Razinkova, D. K. Nadyozhin, and A. D. Dolgov, *Special point on the mass-radius diagram of hybrid stars*, Astronomy Letters **40** (apr, 2014) 201–211, [[arXiv:1404.0865](https://arxiv.org/abs/1404.0865)].

[28] J. M. Lattimer, *The nuclear equation of state and neutron star masses*, Ann.Rev.Nucl.Part.Sci. **62** (2012) 485–515, [[arXiv:1305.3510](https://arxiv.org/abs/1305.3510)].

[29] M. Baldo, ed., *Nuclear Methods and The Nuclear Equation of State*. World Scientific, Singapore, 1999.

[30] B. D. Day, *Three-body correlations in nuclear matter*, Phys. Rev. C **24** (Sep, 1981) 1203–1271.

[31] H. Q. Song, M. Baldo, G. Giansiracusa, and U. Lombardo, *Bethe-brueckner-goldstone expansion in nuclear matter*, Phys. Rev. Lett. **81** (Aug, 1998) 1584–1587.

[32] M. Baldo, A. Fiasconaro, H. Q. Song, G. Giansiracusa, and U. Lombardo, *High density symmetric nuclear matter in the bethe-brueckner-goldstone approach*, Phys. Rev. C **65** (Dec, 2001) 017303.

[33] M. Baldo, A. Polls, A. Rios, H.-J. Schulze, and I. Vidaña, *Comparative study of neutron and nuclear matter with simplified argonne nucleon-nucleon potentials*, Phys. Rev. C **86** (Dec, 2012) 064001.

[34] M. Baldo, I. Bombaci, and G. Burgio, *Microscopic nuclear equation of state with three-body forces and neutron star structure*, Astron.Astrophys. **328** (1997) 274–282, [[astro-ph/9707277](https://arxiv.org/abs/astro-ph/9707277)].

[35] X. R. Zhou, G. F. Burgio, U. Lombardo, H.-J. Schulze, and W. Zuo, *Three-body forces and neutron star structure*, Phys. Rev. C **69** (Jan, 2004) 018801.

[36] R. B. Wiringa, V. G. J. Stoks, and R. Schiavilla, *Accurate nucleon-nucleon potential with charge-independence breaking*, Phys. Rev. C **51** (Jan, 1995) 38–51.

[37] J. Carlson, V. Pandharipande, and R. B. Wiringa, *Three-nucleon interaction in 3-body, 4-body, and infinite-body systems*, Nucl.Phys. **A401** (1983) 59–85.

[38] R. Schiavilla, V. Pandharipande, and R. B. Wiringa, *Momentum distributions in a $A = 3$ and 4 nuclei*, Nucl.Phys. **A449** (1986) 219–242.

[39] Z. H. Li, U. Lombardo, H.-J. Schulze, and W. Zuo, *Consistent nucleon-nucleon potentials and three-body forces*, Phys. Rev. C **77** (Mar, 2008) 034316.

[40] Z. H. Li and H.-J. Schulze, *Nuclear matter with chiral forces in brueckner-hartree-fock approximation*, Phys. Rev. C **85** (Jun, 2012) 064002.

[41] G. Brown, W. Weise, G. Baym, and S. J., *Relativistic Effects in Nuclear Physics*, Comments Nucl.Part.Phys. **17** (1987) 39.

[42] P. M. M. Maessen, T. A. Rijken, and J. J. de Swart, *Soft-core*

baryon-baryon one-boson-exchange models. ii. hyperon-nucleon potential, Phys. Rev. C **40** (Nov, 1989) 2226–2245.

[43] H.-J. Schulze and T. Rijken, *Maximum mass of hyperon stars with the nijmegen esc08 model*, Phys. Rev. C **84** (Sep, 2011) 035801.

[44] Y. Yamamoto, T. Furumoto, N. Yasutake, and T. A. Rijken, *Hyperon mixing and universal many-body repulsion in neutron stars*, Phys. Rev. C **90** (Oct, 2014) 045805.

[45] M. M. Nagels, T. A. Rijken, and Y. Yamamoto, *Extended-soft-core Baryon-Baryon Model Esc08 II. Hyperon-Nucleon Interactions*, arXiv:1501.0663.

[46] I. Vidana, D. Logoteta, C. Providencia, A. Polls, and I. Bombaci, *Estimation of the effect of hyperonic three-body forces on the maximum mass of neutron stars*, Europhys. Lett. **94** (2011) 11002, [arXiv:1006.5660].

[47] M. Baldo, G. F. Burgio, and H.-J. Schulze, *Onset of hyperon formation in neutron star matter from brueckner theory*, Phys. Rev. C **58** (Dec, 1998) 3688–3695.

[48] M. Baldo, G. F. Burgio, and H.-J. Schulze, *Hyperon stars in the brueckner-bethe-goldstone theory*, Phys. Rev. C **61** (Apr, 2000) 055801.

[49] T. Katayama and K. Saito, *Neutron stars with Hyperons in Dirac-Brueckner-Hartree-Fock approach*, arXiv:1410.7166.

[50] A. Di Giacomo, H. G. Dosch, V. Shevchenko, and Y. Simonov, *Field correlators in QCD: Theory and applications*, Phys.Rept. **372** (2002) 319–368, [hep-ph/0007223].

[51] Y. Simonov and M. Trusov, *Deconfinement transition for nonzero baryon density in the field correlator method*, JETP Lett. **85** (2007) 598–601, [hep-ph/0703228].

[52] Y. Simonov and M. Trusov, *Vacuum phase transition at nonzero baryon density*, Physics Letters B **650** (2007), no. 1 36 – 40.

[53] I. Bombaci and D. Logoteta, *A link between measured neutron star masses and lattice QCD data*, Monthly Notices of the Royal Astronomical Society - Letters, Vol. 433, **L79-L83** (2013) [arXiv:1212.5907].

[54] S. Plumari, G. F. Burgio, V. Greco, and D. Zappalà, *Quark matter in neutron stars within the field correlator method*, Phys. Rev. D **88** (Oct, 2013) 083005.

[55] M. Baldo, P. Castorina, and D. Zappalà, *Gluon condensation and deconfinement critical density in nuclear matter*, Nucl.Phys. **A743** (2004) 3–12, [nucl-th/0311038].

[56] M. Baldo, G. F. Burgio, P. Castorina, S. Plumari, and D. Zappalà, *Astrophysical constraints on the confining models: The field correlator method*, Phys. Rev. D **78** (Sep, 2008) 063009.